



CHORUS

This is the accepted manuscript made available via CHORUS. The article has been published as:

Magnetolectric excitations in multiferroic Ni₃TeO₆

Stella Skiadopoulou, Fedir Borodavka, Christelle Kadlec, Filip Kadlec, Maria Retuerto, Zheng Deng, Martha Greenblatt, and Stanislav Kamba

Phys. Rev. B **95**, 184435 — Published 30 May 2017

DOI: [10.1103/PhysRevB.95.184435](https://doi.org/10.1103/PhysRevB.95.184435)

Magnetolectric excitations in multiferroic Ni_3TeO_6

Stella Skiadopoulou,¹ Fedir Borodavka,¹ Christelle Kadlec,¹ Filip Kadlec,¹ Maria Retuerto,² Zheng Deng,² Martha Greenblatt² and Stanislav Kamba^{1,*}

¹*Institute of Physics, Czech Academy of Sciences, Na Slovance 2, 18221 Prague 8, Czech Republic*

²*Department of Chemistry and Chemical Biology, Rutgers, The State University of New Jersey, 610 Taylor Road, Piscataway, NJ 08854, USA*

The spin-order-induced ferroelectric anti-ferromagnet Ni_3TeO_6 transcends the magnetolectric performance of all other single-phase multiferroics, because it exhibits non-hysteretic colossal magnetolectric coupling [Oh *et al.*, Nat. Commun., 5, 3201 (2014)]. We investigated spin and lattice excitations in Ni_3TeO_6 by a combination of infrared, Raman and THz spectroscopies. Two spin excitations (near 13 and 35 cm^{-1}) were observed simultaneously in Raman and time-domain THz spectra below the Néel temperature $T_N=53$ K. We propose to assign them to electromagnons, which are activated by the dynamic magnetolectric coupling. A third magnon is seen only in the Raman spectra near 206 cm^{-1} .

I. INTRODUCTION

The high demands for energy and cost efficiency of the technological world have led to the necessity of multifunctional devices. Magnetolectric multiferroics are strong candidates for such novel applications owing to the potential use of electrical field to tune their magnetic properties.^{1,2}

However, only a few single-phase multiferroics manifest a strong magnetolectric coupling³⁻⁷ and all those materials are type-II multiferroics, where the ferroelectric polarization is spin-order-induced.^{3-6,8} Among them, only Ni_3TeO_6 exhibits a non-hysteretic colossal magnetolectric effect. However, this occurs only at magnetic fields near 8.5 T⁶ and 53 T,⁹ where spin-flop and metamagnetic phase transitions occur, respectively. The absence of hysteretic behavior in the magnetic-field dependence of magnetization and ferroelectric polarization precludes losses, which is highly promising for a number of magnetolectric applications.

At room temperature, Ni_3TeO_6 has a corundum-related structure with the polar R3 space group.^{10,11} A collinear antiferromagnetic (AFM) order appears below $T_N=53$ K,¹² giving

rise to a spin-induced ferroelectric ordering.⁶ The previous report of a ferroelectric phase transition at 1000 K¹³ is questionable, because the reported dielectric dispersion is typical of the Maxwell-Wagner relaxation in conducting systems,¹⁴ and no switchable ferroelectric polarization has been observed above 53 K. Lattice dynamics of Ni_3TeO_6 were investigated above 150 cm^{-1} using infrared (IR) spectroscopy as a function of temperature and magnetic field.¹⁵ Phonon anomalies due to spin-phonon coupling were observed near T_N and a spin-flop transition close to 9 T, but also near 30 T, which suggest another magnetic phase transition at 30 T.¹⁵ In addition, interlocked chiral and polar domain walls were observed at room temperature, unveiling a complex coupling between the chiral and polar order parameters.¹⁶

Due to sum rules, the static magnetolectric coupling should be governed by magnetolectric excitations (electromagnons) in the GHz and/or THz regions.¹⁷ These spin excitations can contribute to the dynamic magnetolectric coupling between the magnetic permeability and dielectric permittivity, and if the magnetic structure is sensitive to the static magnetic or electric field, the electromagnons can be tuned by these fields.^{18,19} The possibility to modulate the index of refraction could promote the design of novel optoelectronic devices. Since

* Corresponding author: kamba@fzu.cz

electromagnons very often lie in the THz range of the electromagnetic spectrum, THz spectroscopy is an essential tool for detecting such excitations. However, a combination of spectroscopic techniques are required to account for the nature of the detected excitations, since the spin excitations can be pure magnons (contributing only to the magnetic permeability μ) or electromagnons (contributing also to the permittivity ϵ^*). Polarized THz or IR spectroscopy of single crystals is commonly used for distinguishing between magnons and electromagnons,^{9,17,20} but, to this aim, all possible polarized spectra or the directional dichroism should be measured. Such experiments require relatively large single crystals with dimensions of the order of several millimeters, which are often unavailable. Since each polar excitation should be both IR and Raman active in a non-centrosymmetric ferroelectric phase,²¹ the combination of both these techniques can be used for identifying the electromagnons even in polycrystalline samples.

In that fashion, we studied Ni_3TeO_6 single crystals and ceramics by Fourier-Transform IR, Raman and time-domain THz spectroscopies, in a temperature range between 4 and 300 K. We show that Ni_3TeO_6 exhibits dynamic magnetoelectric coupling, inducing at least 2 excitations simultaneously detected by Raman and THz spectroscopy, interpreted as electromagnons.

II. EXPERIMENTAL DETAILS

Ni_3TeO_6 was prepared as polycrystalline powders and single crystals. Green Ni_3TeO_6 powders were synthesized by solid state methods from stoichiometric amounts of analytical-grade NiO and TeO_2 , and heating the mixture at 800 °C for 12 hours in O_2 flow. The single crystals were grown from a flux composed of the previously prepared powders of Ni_3TeO_6 , V_2O_5 , TeO_2 , NaCl and KCl in a molar ratio of 1:5:10:10:5. The mixture was heated for three days at 830°C and then cooled down to 600°C during five days. Plate-shaped green single crystals ~2 mm in diameter and with thickness 60-100 μm were obtained.

Near-normal incidence IR reflectivity spectra of the Ni_3TeO_6 ceramics were measured by a Fourier-transform IR spectrometer Bruker IFS 113v in the frequency range of 20—3000 cm^{-1} (0.6 – 90 THz) at room temperature (RT); for the low-temperature measurements the spectral range

was reduced by the transparency of cryostat windows to 20—650 cm^{-1} . A pyroelectric deuterated triglycine sulfate detector was used for the room-temperature measurements, whereas a He-cooled (operating temperature 1.6 K) Si bolometer was used for the low-temperature measurements down to 7 K.

THz measurements from 3 to 60 cm^{-1} (0.09 – 1.8 THz) were performed in the transmission geometry with a custom-made time-domain terahertz spectrometer. In this spectrometer, a femtosecond Ti:sapphire laser oscillator (Coherent, Mira) produces a train of femtosecond pulses, which generate linearly polarized broadband THz pulses radiated by a photoconducting switch TeraSED (Giga-Optics). A gated detection scheme based on electrooptic sampling with a 1 mm thick [110] ZnTe crystal as a sensor allows us to measure the time profile of the electric field of the transmitted THz pulse. Two Oxford Instruments Optistat optical cryostats with mylar and polyethylene windows were used for low-temperature THz and IR measurements, respectively. THz experiments in an external magnetic field $H_{\text{ext}} \leq 7$ T were performed with an Oxford Instruments Spectromag cryostat in the Voigt configuration, where the electric component of the THz radiation E_{THz} was set parallel and perpendicular to H_{ext} .

The IR reflectivity and THz complex permittivity spectra were fitted assuming a sum of N independent three-parameter damped harmonic oscillators, expressed as:²²

$$\epsilon^*(\omega) = \epsilon_\infty + \sum_{j=1}^N \frac{\Delta\epsilon_j \omega_{\text{TO}j}^2}{\omega_{\text{TO}j}^2 - \omega^2 + i\omega\gamma_{\text{TO}j}} \quad (1)$$

where $\Delta\epsilon_j$ is the dielectric strength of the j -th mode, $\omega_{\text{TO}j}$ the frequencies of the j -th transverse optical (TO) phonons, and $\gamma_{\text{TO}j}$ are the corresponding damping constants. ϵ_∞ is the high-frequency (electronic) contribution to the permittivity, determined from the room-temperature frequency-independent reflectivity tail above the phonon frequencies. The reflectivity $R(\omega)$ is related to the complex dielectric function $\epsilon^*(\omega)$ by:

$$R(\omega) = \left| \frac{\sqrt{\epsilon^*} - 1}{\sqrt{\epsilon^*} + 1} \right|^2 \quad (2)$$

For Raman studies of single crystals, a Renishaw RM 1000 Micro-Raman spectrometer with Bragg filters was used, equipped with an Oxford Instruments Microstat continuous-flow optical He cryostat. The experiments were performed in the backscattering geometry in the

5–1800 cm^{-1} range. An Ar^+ -ion laser operating at 514.5 nm was used. The spectra were carefully fitted with the sum of independent damped harmonic oscillators multiplied by the corresponding Stokes temperature factor.²³

III. RESULTS

A. Lattice excitations in Ni_3TeO_6

The IR reflectivity spectra of the Ni_3TeO_6 ceramics for selected temperatures from 7 to 300 K are shown in Fig. 1(a). We present the spectra only from 150 cm^{-1} , because other weak excitations are seen only below 40 cm^{-1} and these are better resolved in the THz spectra, which will be discussed below. As predicted by the factor group analysis for the crystal structure with R3 symmetry,^{10,11} 9 $E(x,y,x^2-y^2,xy,xz,yz)$ and 9 $A(x^2+y^2,z^2,z)$ modes are expected, both IR and Raman active.¹⁵ All 18 modes can be seen in the IR spectra up to 300 K.

No significant changes in phonon eigenfrequencies and/or respective damping are observable as a function of temperature, apart from the expected decrease on damping upon cooling. The spectra reveal similar mode frequencies as the previously studied Ni_3TeO_6 ,¹⁵ with 10 of the modes seen above 360 cm^{-1} corresponding to the vibrations of the TeO_6 octahedra.²⁴ Since there is no change of crystal symmetry at the AFM phase transition, no change in phonon selection rules is expected. The phonon parameters obtained from the IR spectra fits are listed in TABLE 1, together with the frequencies reported by Yokosuk *et al.*¹⁵ and with phonon frequencies obtained from our polarized Raman spectra of the single crystal.

The complex permittivity calculated from IR spectra fits is presented in Fig. 1(b) and (c). One can notice that the static permittivity $\epsilon(0)$ attains a value of ca. 4.5 only, which is common among the spin-induced ferroelectrics. This value is also in agreement with the very low IR reflectivity values and with the THz spectra (Fig. 4), and it can be viewed as a consequence of the low Born effective charges of all lattice vibrations. The difference between our static permittivity and its value of nearly 11 observed in the radio-frequency region by Oh *et al.*⁶ could be explained by the high porosity of our ceramics (about 58%) and/or by the existence of another dielectric relaxation in the microwave region.

In the inset of Fig. 1(b), the mode around 310 cm^{-1} shows a remarkable increase in intensity

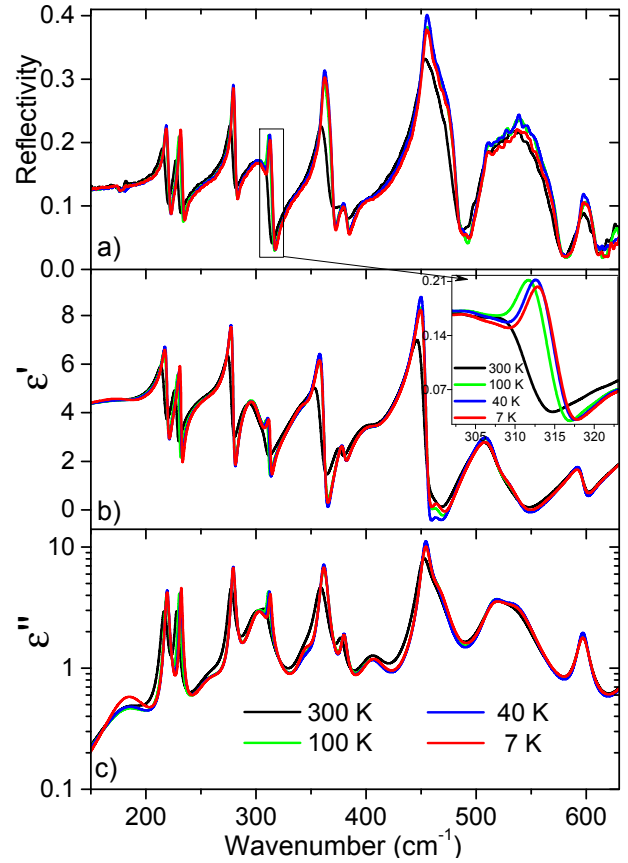


Figure 1 (a) Experimental IR reflectivity spectra of Ni_3TeO_6 ceramics at selected temperatures from 7 to 300 K. (b) Real and (c) imaginary parts of permittivity, as obtained from the fits. Inset: Temperature dependence of IR reflectivity of the mode around 310 cm^{-1} showing, on cooling, a marked decrease in its damping, accompanied by a frequency increase (hardening).

upon cooling towards 40 K due to a decrease in phonon damping, accompanied by a slight hardening. Below $T_N \approx 53$ K, the same phonon exhibits a small decrease in intensity. Since the structure displays no anomaly at T_N , this is probably linked to the transfer of its dielectric strength to a lower-energy spin excitation appearing in the THz spectra in the AFM phase. The anomalous temperature behavior of this mode was reported by Yokosuk *et al.*,¹⁵ who observed its hardening by 2.5 cm^{-1} on cooling down to T_N and its softening below T_N , which they explained by spin-phonon coupling.

We measured polarized Raman back-scattering spectra of the Ni_3TeO_6 single crystals in all possible polarization configurations and at temperatures from 4 to 300 K. Raman spectra measured in four polarization configurations at 4 K are shown in Fig. 2. The temperature dependence of the cross-polarized $z(xy)\bar{z}$ Raman spectra (according to the Porto notation)²⁵ can be seen in Fig. 3, where 13 phonons were observed.

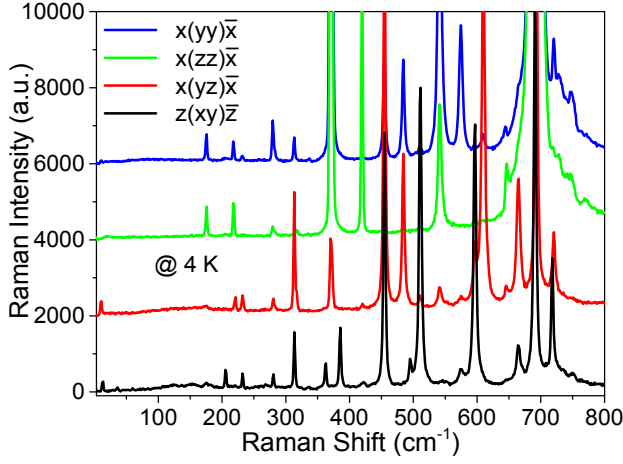


Figure 2 Raman spectra of the Ni_3TeO_6 single crystal collected at different polarization configurations at 4 K.

In the notation followed in this paper x , y and z directions are mutually perpendicular; z direction is parallel to the hexagonal c -axis, while x and y directions are lying in the ab -plane. The combination of $x(zz)\bar{x}$ and $z(xy)\bar{z}$ reveals all 18 predicted modes. The eigenfrequencies of different configurations ($x(yy)\bar{x}$, $x(yz)\bar{x}$, $x(zz)\bar{x}$ and $z(xy)\bar{z}$), together with the respective symmetry assignment, are listed in TABLE 1, which provides their comparison with the polar phonon frequencies obtained from our IR spectra. The frequencies of Raman and IR modes correspond to each other, confirming the prediction of the factor group analysis that these modes should have the same symmetry. **Five $A(LO)$ -symmetry modes near 179, 385, 495, 691 and 720 cm^{-1} , which are allowed in $z(xx)\bar{z}$ spectra, appear as well in the $z(xy)\bar{z}$ spectra (E symmetry), possibly due to polarization leakage.** Such mode mixing could be attributed to sample misalignment, crystal imperfections or depolarization effect.^{26–28} Note that two modes observed in the IR spectra were not seen in any of the Raman spectra.

Below 210 cm^{-1} , in the AFM phase, a number of new modes are activated in the $z(xy)\bar{z}$ Raman spectra. Among them, the mode near 206 cm^{-1} becomes very sharp and intense on cooling, whereas the mode activated on the low-frequency edge of our spectra at 9.9 cm^{-1} (40 K) hardens on cooling to 12.7 cm^{-1} (4 K). These modes, together with other ones resolved below 200 cm^{-1} , cannot be new phonons, because the space group $R3$ does not change below T_N . These must be spin excitations. This conclusion will be confirmed below, because two modes seen below 40 cm^{-1} in the THz transmission spectra are highly sensitive to external magnetic field. Lastly, the weak

modes between 130 and 190 cm^{-1} originate probably in multimagnon scattering.

B. Electromagnons in Ni_3TeO_6

In order to investigate the far-IR domain, we measured time-domain THz spectra of Ni_3TeO_6 ceramics (crystals were too small) in a temperature range from 10 to 300 K in an external magnetic field \mathbf{H}_{ext} up to 7 T. The THz spectra for selected temperatures and magnetic fields are shown in Fig. 4. Both configurations with $\mathbf{H}_{\text{ext}} \parallel \mathbf{E}_{\text{THz}}$ and $\mathbf{H}_{\text{ext}} \perp \mathbf{E}_{\text{THz}}$ were measured, and both orientations reveal similar features. Here we present only the latter spectra.

The THz spectra were fitted together with the IR ones, according to the model mentioned above. Two spin excitations are clearly seen in both real and imaginary parts of the refractive index spectra, corresponding to frequencies of approximately 16 and 32 cm^{-1} , at 7 K (see TABLE 1). These two modes are not active above T_N . **Upon cooling, one weak and broad excitation appears at 48 K near 25 cm^{-1} and hardens to 32 cm^{-1} . Another sharp mode activates near 16 cm^{-1} .**

This excitation markedly softens with \mathbf{H}_{ext} . Unfortunately, we could use magnetic field only up to 7 T, so we could not see the influence of the

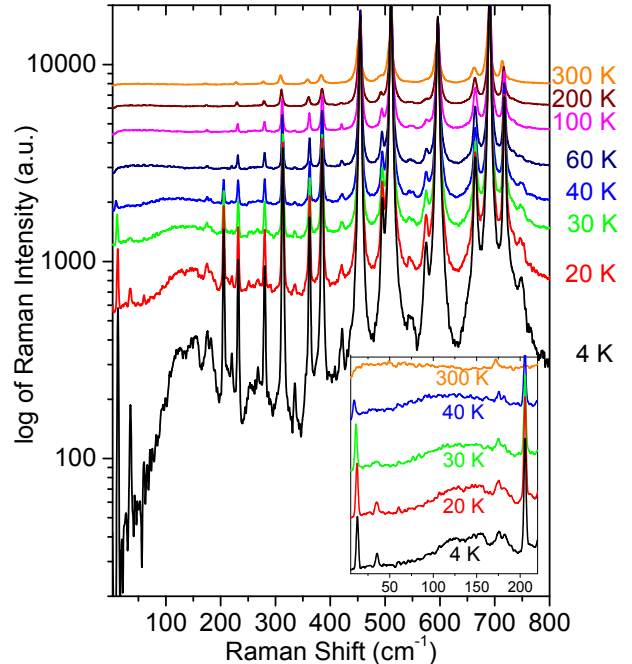


Figure 3 Temperature dependence of $z(xy)\bar{z}$ Raman spectra of the Ni_3TeO_6 single crystal. Inset: Detail of the lower spectral range, where the two spin excitation modes around 12 and 35 cm^{-1} appear below 45 K, and harden upon cooling. The activation of other modes up to 206 cm^{-1} is discussed in the text.

TABLE 1. Frequencies of the IR active modes in the Ni_3TeO_6 ceramics at 7 K and Raman active modes in Ni_3TeO_6 single crystal at 4 K, as obtained by the fits of IR reflectivity with $\epsilon_\infty = 2.2$. The first column corresponds to the IR mode frequencies (300 K) from Yokosuk *et al.*¹⁵ Apart from the frequency, we list the damping constants and dielectric strength of the IR-active modes. The LO modes observed in Raman spectra are marked by + in superscript.

ω_{TO}^{15}	Symmetry	Raman 4 K				IR 7 K		
		$x(yy)\bar{x}$ $\omega_{\text{TO}}(\text{cm}^{-1})$	$x(yz)\bar{x}$ $\omega_{\text{TO}}(\text{cm}^{-1})$	$x(zz)\bar{x}$ $\omega_{\text{TO}}(\text{cm}^{-1})$	$z(xy)\bar{z}$ $\omega_{\text{TO}}(\text{cm}^{-1})$	$\omega_{\text{TO}}(\text{cm}^{-1})$	$\gamma_{\text{TO}}(\text{cm}^{-1})$	$\Delta\epsilon$
--	electromagnon		10.5		12.7	16.2	2.1	0.004
--	electromagnon				35.3	32.4	8.3	0.007
171	A	176.0		176.0	179.4 ⁺	185.0	46.4	0.12
--	(electro)magnon				205.6			
214	A	217.5		217.5		219.3	4.4	0.08
217	E		220.6		220.5			
228	E				232.0	232.1	2.6	0.05
--						259.2	37.0	0.07
278	E				280.4	279.3	4.2	0.09
278	A	279.6		279.7		303.1	24.2	0.21
310	E	313.5	313.4		313.2	313.2	3.1	0.02
--	A			317.0		345.2	17.8	0.04
360	E				362.2	361.7	8.3	0.14
370	A	370.0		370.0		380.0	6.7	0.02
--					385.1 ⁺			
451	A			419.1		406.6	30.0	0.06
456	E	454.7	454.9		454.5	454.2	10.0	0.18
--		484.3 ⁺	484.5 ⁺		494.8 ⁺	466.1	23.2	0.15
513	E		510.7		510.7	516.5	27.4	0.11
541	A	540.9	541.8	542.0		536.6	41.3	0.18
597	E	574.8 ⁺	609.5 ⁺		596.1	597.1	13.7	0.03
649	A			646.9				
666	E		664.9		664.0	661.2	25.0	0.10
692	A	693.0	693.0	693.0	690.5 ⁺	690.5	45.4	0.06
--			720.4 ⁺		717.7 ⁺			

spin flop transition occurring at approximately 8 T on the mode frequencies. The second mode seen near 32 cm^{-1} seems to exhibit splitting upon applying \mathbf{H}_{ext} , but it is not well resolved, because the sample is polycrystalline. Since both excitations activate only below T_N and their frequencies are sensitive to magnetic field, these must be spin excitations.

In order to compare the results of the two distinct spectroscopic techniques, we present in Fig. 4(c) the Raman spectra in the low-frequency region at temperatures up to 45 K. The frequencies of the two spin excitations in Raman spectra are approximately 13 and 35 cm^{-1} in the single crystal, whereas those observed in the ceramics by time-domain THz experiments amount to 16 and 32 cm^{-1} . If we take into account the different crystallinity of the samples, such discrepancies lie within the experimental error,

therefore we assert that both experiments reveal the same pair of excitations and we propose that these are electromagnons. Magnons are usually extremely weak in Raman spectra, but if a magnon becomes electrically active, it can be stronger and it should follow the same IR and Raman selection rules in polar crystal structure.²² Since the electromagnons are active in xy Raman spectra, they must have E symmetry.

Below T_N , another sharp and strong excitation activates in $z(xy)\bar{z}$ Raman spectra at 206 cm^{-1} (Fig. 3). It probably also has a spin origin and, because it has E symmetry, it could also be an electromagnon. Nevertheless, this mode is resolved in neither our nor previous¹⁶ IR studies, so we cannot confirm its polar character.

IV. DISCUSSION

Ni_3TeO_6 has a polar $R3$ structure at least up to 1000 K,¹⁴ and its non-switchable polarization must be, due to the space group symmetry, oriented along the c axis. Below T_N , the exchange striction ($\propto \mathbf{S}_i \cdot \mathbf{S}_j$) between collinear spins of Ni cations changes the bond lengths between these atoms.⁷ The question arises whether Ni_3TeO_6 is truly ferroelectric, or rather merely pyroelectric with a spontaneous polarization which is just influenced by the magnetic order. The second scenario is also supported by the experimental fact that the external magnetic field *reduces* the spontaneous polarization and this polarization change is most remarkable at the spin flop transition near 9 T.⁷

Our electromagnons have the E symmetry, because they are active in the $x(\bar{z}z)\bar{x}$ and $z(xy)\bar{z}$ polarized Raman spectra, and therefore they must be IR active in the $E \perp z$ spectra. Since the spontaneous static polarization is oriented along z axis and the electromagnons are polarized perpendicularly to this direction, the spin excitations become electrically active due to dynamic fluctuations of spins (and the related polarization) out of the z axis. This dynamic polarization can be induced by the same exchange striction mechanism as the static polarization. Generally, electromagnons must receive their dielectric strength from polar phonons of the same symmetry. In Ni_3TeO_6 Yokosuk et al.¹⁵ observed 3 IR-active phonons of E symmetry (at 310, 597 and 668 cm^{-1}) exhibiting anomalies at T_N , while no A -symmetry phonon exhibited any anomaly at the AFM phase transition. As discussed earlier, we observed frequency hardening and an intense decrease in the damping of the 310 cm^{-1} mode on cooling, however, no trace of anomaly was seen for the higher frequency modes (597 and 668 cm^{-1}). Therefore, the electromagnons are coupled with the E -symmetry phonon near 310 cm^{-1} . The above-mentioned anomalous E phonons are related to stretching or bending of the octahedral cages of TeO_6 and NiO_6 inducing a further modulation of the superexchange interaction between the Ni ions along the c -axis.¹⁵

Even though polycrystalline ceramic samples were used for the THz experiments, the electromagnons are still reasonably sharp. Unfortunately, the size of the single-crystalline samples (≤ 1 mm diameter) was not sufficient for the IR and THz spectroscopies, since large and well-polished surfaces are needed for these

techniques. Studying oriented single-crystalline samples by THz spectroscopy would help to confirm the E -symmetry and polar character of the electromagnons, and the possible directional

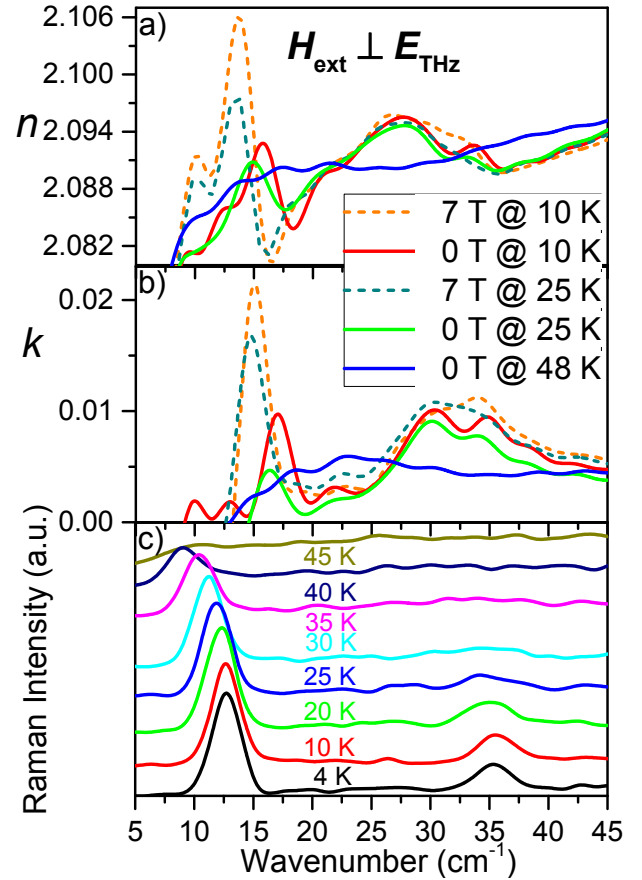


Figure 4 Temperature dependence of (a) real and (b) imaginary part of index of refraction, as obtained by the THz measurements at $H_{\text{ext}} \perp E_{\text{THz}}$ for the Ni_3TeO_6 ceramics. Two excitations appear below 48 K (close to $T_N \approx 53$ K). Upon application of H_{ext} up to 7 T, softening of the lowest frequency mode is observed. (c) Temperature evolution of $z(xy)\bar{z}$ Raman spectra of the Ni_3TeO_6 single crystal below 45 K.

dichroism could be investigated. In addition, splitting of electromagnons in an external magnetic field might be observed.

One can argue that the dielectric strengths of the electromagnons should enhance ϵ' below T_C , however, such behavior was not observed in the temperature dependence of ϵ' reported in ref. [6]. This is due to the low dielectric strength of both electromagnons ($\Delta\epsilon_1 + \Delta\epsilon_2 = 0.011$ at 7 K – see Table 1) which cannot be resolved in $\epsilon'(T)$. Note that $\epsilon'(T)$ exhibits only a small peak at T_C (increase by ~ 0.15) and this dielectric anomaly can be caused by softening of the electromagnons down to the microwave range near T_C . A similar

effect was recently observed in the multiferroic MnWO_4 by Niermann *et al.*²⁹

Lastly, we performed Raman studies of the Ni_3TeO_6 single crystal in an external electrical field parallel to the c -axis (up to 60 kV/cm), in order to investigate the behavior of the electromagnons on external bias. However, no significant effect was observed. Bad quality of contact electrodes, non-uniformly applied electrical field and/or defects in the crystal may have hindered our efforts for such observation.

V. CONCLUSION

To conclude, we studied the dynamic magnetoelectric coupling in the multiferroic Ni_3TeO_6 by a combination of IR, Raman and time-domain THz spectroscopic techniques. A thorough investigation of lattice and spin excitations was conducted by Raman spectroscopy of single crystals, measuring all possible polarization configurations, and reported for the first time in literature. At least two spin excitations around $15\pm 2\text{ cm}^{-1}$ and 35 cm^{-1} appear simultaneously in the AFM phase in both THz and Raman spectra, thus corresponding to electromagnons. The lowest-frequency electromagnon displays a strong sensitivity at external magnetic field, by increasing its intensity

and decreasing its frequency. Another sharp excitation appears below T_N near 206 cm^{-1} . Since it is not resolved in unpolarized IR reflectivity spectra of ceramics, we assume it is a magnon. Nevertheless, we cannot exclude that it is also an electromagnon, which would be screened by a stronger A -symmetry polar phonon near 219 cm^{-1} . Further studies of Ni_3TeO_6 single crystals by polarized time-domain THz spectroscopy are required for a detailed polarization analysis of electromagnons, a possible detection of a directional dichroism, and for determining the dependence of the electromagnon frequency on the external magnetic field strength (including a possible splitting). A better understanding of the electromagnonic behavior can lead to a deeper insight into the mechanisms of dynamic magnetoelectric coupling in multiferroics.

Acknowledgements

This work was supported by European Union funding under the 7th Framework Programme (Project NOTEDEV), by the Czech Science Foundation (Project 15-08389S) and MŠMT KONTAKT II project LH15122. The work of MG, ZD and MR was supported by NSF-DMR-1507252 grant.

¹ M. Fiebig, J. Phys. D. Appl. Phys. **38**, R123 (2005).

² W. Eerenstein, N.D. Mathur, and J.F. Scott, Nature **442**, 759 (2006).

³ T. Aoyama, K. Yamauchi, A. Iyama, S. Picozzi, K. Shimizu, and T. Kimura, Nat. Commun **5**, 4927 (2014).

⁴ S.H. Chun, Y.S. Chai, Y.S. Oh, D. Jaiswal-Nagar, S.Y. Haam, I. Kim, B. Lee, D.H. Nam, K.-T. Ko, J.-H. Park, J.-H. Chung, and K.H. Kim, Phys. Rev. Lett. **104**, 37204 (2010).

⁵ N. Lee, C. Vecchini, Y.J. Choi, L.C. Chapon, A. Bombardi, P.G. Radaelli, and S.-W. Cheong, Phys. Rev. Lett. **110**, 137203 (2013).

⁶ Y.S. Oh, S. Artyukhin, J.J. Yang, V. Zapf, J.W. Kim, D. Vanderbilt, and S.-W. Cheong, Nat Commun **5**, 3201 (2014).

⁷ Y.S. Chai, S. Kwon, S.H. Chun, I. Kim, B.-G. Jeon, K.H. Kim, and S. Lee, Nat. Commun **5**, (2014).

⁸ Y. Tokura, S. Shinichiro, and N. Naoto, Reports Prog. Phys. **77**, 76501 (2014).

⁹ J.W. Kim, S. Artyukhin, E.D. Mun, M. Jaime, N. Harrison, A. Hansen, J.J. Yang, Y.S. Oh, D. Vanderbilt, V.S. Zapf, and S.-W. Cheong, Phys. Rev. Lett. **115**, 137201 (2015).

¹⁰ R.E. Newnham and E.P. Meagher, Mater. Res.

Bull. **2**, 549 (1967).

¹¹ R. Becker and H. Berger, Acta Crystallogr. Sect. E **62**, 222 (2006).

¹² I. Živković, K. Prša, O. Zaharko, and H. Berger, J. Phys. Condens. Matter **22**, 56002 (2010).

¹³ S.A. Ivanov, R. Mathieu, P. Nordblad, R. Tellgren, C. Ritter, E. Politova, G. Kaleva, A. Mosunov, S. Stefanovich, and M. Weil, Chem. Mater. **25**, 935 (2013).

¹⁴ P. Lunkenheimer, S. Krohns, S. Riegg, S.G. Ebbinghaus, A. Reller, and A. Loidl, Eur. Phys. J. Spec. Top. **180**, 61 (2009).

¹⁵ M.O. Yokosuk, S. Artyukhin, A. Al-Wahish, X. Wang, J. Yang, Z. Li, S.-W. Cheong, D. Vanderbilt, and J.L. Musfeldt, Phys. Rev. B **92**, 144305 (2015).

¹⁶ X. Wang, F.-T. Huang, J. Yang, Y.S. Oh, and S.-W. Cheong, APL Mater. **3**, 76105 (2015).

¹⁷ D. Szaller, S. Bordács, V. Kocsis, T. Rődöm, U. Nagel, and I. Kézsmárki, Phys. Rev. B **89**, 184419 (2014).

¹⁸ A. Pimenov, A.A. Mukhin, V.Y. Ivanov, V.D. Travkin, A.M. Balbashov, and A. Loidl, Nat Phys **2**, 97 (2006).

¹⁹ P. Rovillain, R. de Sousa, Y. Gallais, A. Sacuto, M.A. Méasson, D. Colson, A. Forget, M. Bibes, A. Barthélémy, and M. Cazayous, Nat Mater **9**, 975

(2010).

²⁰ S. Dong, J.-M. Liu, S.-W. Cheong, and Z. Ren, *Adv. Phys.* **64**, 519 (2015).

²¹ S. Skiadopoulou, V. Goian, C. Kadlec, F. Kadlec, X.F. Bai, I.C. Infante, B. Dkhil, C. Adamo, D.G. Schlom, and S. Kamba, *Phys. Rev. B* **91**, 174108 (2015).

²² F. Gervais, in *Chap. 7 High-Temperature Infrared Reflectivity Spectrosc. by Scanning Interf. Vol. 8 Infrared Millim. Waves*, edited by K.J. Button (Academic, New York, 1983), p. 279.

²³ M. Tyunina, A. Dejneka, D. Rytz, I. Gregora, F. Borodavka, M. Vondracek, and J. Honolka, *J. Phys. Condens. Matter* **26**, 125901 (2014).

²⁴ G. Blasse and W. Hordijk, *J. Solid State Chem.* **5**, 395 (1972).

²⁵ T.C. Damen, S.P.S. Porto, and B. Tell, *Phys. Rev.* **142**, 570 (1966).

²⁶ G. Turrell, *J. Raman Spectrosc.* **15**, 103 (1984).

²⁷ C. Bremard, P. Dhamelincourt, J. Laureyns, and G. Turrell, *Appl. Spectrosc.* **39**, 1036 (1985).

²⁸ H. Morishita, Y. Hoshino, S. Higuchi, F. Kaneko, K. Tashiro, and the late M. Kobayashi, *J. Raman Spectrosc.* **31**, 455 (2000).

²⁹ D. Niermann, C.P. Grams, P. Becker, L. Bohatý, H. Schenck, and J. Hemberger, *Phys. Rev. Lett.* **114**, 37204 (2015).